Coronagraphic wavefront control for the ATLAST-9.2m telescope

Richard G. Lyon*[a], William R. Oegerle[a], Lee D. Feinberg[a], Matthew R. Bolcar[a], Bruce H. Dean[a], Gary E. Mosier[a], Marc Postman[b]
[a]NASA Goddard Space Flight Center, Greenbelt, MD, USA 20771
[b]Space Telescope Science Institute, Baltimore, MD, USA 21218

ABSTRACT

The Advanced Technology for Large Aperture Space Telescope (ATLAST) concept was assessed as one of the NASA Astrophysics Strategic Mission Concepts (ASMC) studies. Herein we discuss the 9.2-meter diameter segmented aperture version and its wavefront sensing and control (WFSC) with regards to coronagraphic detection and spectroscopic characterization of exoplanets. The WFSC would consist of at least two levels of sensing and control: (i) an outer coarser level of sensing and control to phase and control the segments and secondary mirror in a manner similar to the James Webb Space Telescope but operating at higher temporal bandwidth, and (ii) an inner, coronagraphic instrument based, fine level of sensing and control for both amplitude and wavefront errors operating at higher temporal bandwidths. The outer loop would control rigid-body actuators on the primary and secondary mirrors while the inner loop would control one or more segmented deformable mirror to suppress the starlight within the coronagraphic field-of-view. Herein we discuss the visible nulling coronagraph (VNC) and the requirements it levies on wavefront sensing and control and show the results of closed-loop simulations to assess performance and evaluate the trade space of system level stability versus control bandwidth.

Keywords: Large space telescopes, segmented telescopes, coronagraph, wavefront sensing, wavefront control

1. INTRODUCTION

The Advanced Large Aperture Space Telescope (ATLAST) is a mission concept for a NASA astrophysics mission beyond 2020 and would operate in the ultraviolet (UV), optical and near-infrared (NIR). ATLAST-9.2m would consist of a 9.2 meter segmented primary mirror diameter and be diffraction limited at λ=500 nm, yielding angular resolution (λ/D) of ~13 milli-arcseconds in visible light. The wide span of science enabled by ATLAST is described in ASMC final report[1] and available from http://www.stsci.edu/institute/atlast. One of ATLAST's science goals is the detection of earth-mass exoplanets and characterization of their atmospheres, and the surrounding parents star's dust and debris disk. This requires coronagraphy to increase the contrast of the planet relative the parent star. Coronagraphy is ultimately limited by the diffracted, scattered and stray light leaked through the optical system to the coronagraphic focal plane and it is this light which must be sensed and controlled.

A multitude of coronagraphic approaches exist of which only two are known to be viable options for a segmented aperture telescope: (i) an external occulter[2], and (ii) a visible nulling coronagraph[3]. An external occulter suppresses the starlight prior to entering the telescope making the requirements on the telescope collection system more benign, however, it comes at expense of flying two separate spacecraft separated by > 10,000 km where the 2nd spacecraft is a large deployable occulter (~50 m or larger) with tolerances on its shape of ~100 microns[2]. External occulter approaches have been studied for the Hubble Space Telescope (HST), James Webb Space Telescope (JWST), and as part the ASMC studies and for ATLAST. Herein we assess the use of the 2nd option, i.e. the visible nulling coronagraph (VNC). A VNC has been studied by NASA for the Extrasolar Planetary Imaging Coronagraph[4,5] (EPIC) and for the Dilute Aperture Visible Nulling Coronagraphic Imager[6] (DAViNCI) ASMC studies and multiple ground testbeds[7,8,9] are in various stages of development to assess performance and develop sensing and control approaches for the VNC and its associated technologies.

*richard.g.lyon@nasa.gov; phone 1 301 286-4302

2. OVERVIEW OF ATLAST-9.2M

2.1 Optical Telescope Element (OTE)

ATLAST-9.2m consists of a deployed optical system whereby the primary mirror (PM) and the secondary mirror (SM) and its tower fold up to a stowed configuration to enabling it to fit into the a 6.5m fairing of a Delta-IV Heavy version of the Evolved Expendable Launch Vehicle (EELV). The stowed and deployed configurations are shown on the left- and right-panels of figure-1 respectively.

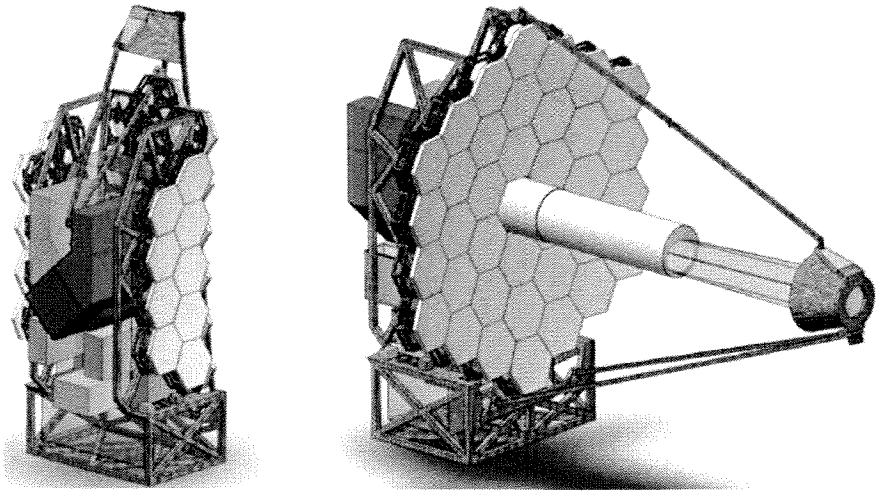

Figure-1: Stowed and deployed configurations of ATLAST-9.2m

The optical configuration is a three mirror anastigmat (TMA) with the PM consisting of 36 hexagonal ULE glass segments, width per segment is 1.315 meters flat-to-flat. The segments are hexagonal packed with the center segment missing to allow light from the SM to pass through the center of the PM and into the instruments residing behind the primary mirror. A large deployed sunshield keeps sunlight off the telescope and its support structure. Each segment is mounted on a hexapod which gives 6 degree of freedom (DOF) rigid body control per segment and additionally a radius of curvature force actuator allows deformation of segment to changes its radius of curvature, yielding 7 DOF per segment. Additionally the SM is mounted on a hexpod (6 DOF) that is mounted on three support struts coupled back to the PM backplane supporting structure. Thus the OTE has 36 x 7 + 6 = 258 controllable DOF and has legacy to the JWST. The larger areal density ULE was baselined, over JWST's Beryllium, since ATLAST-9.2m will operate at room temperature and requires greater stiffness for higher wavefront quality – a significant consideration for coronagraphy.

The aperture thus consists of a hexagonal region of 9.2 meters from outer flat edge to out flat edge with a 3 obscurations for the struts and a central hole as shown in figure-2.

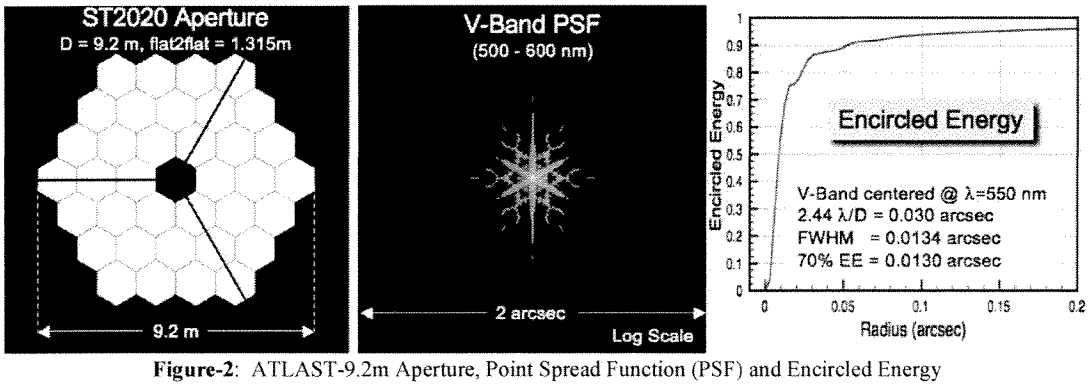

Figure-2: ATLAST-9.2m Aperture, Point Spread Function (PSF) and Encircled Energy

Table-1: System Level Parameters and Coarse & Fine Wavefront Control

	Parameter	Value	Comments
System	Telescope Configuration	9.2 m on-axis segmented	w/ SM obscuration, 3 SM struts, TMA
	Segments	36 hex, 1.315 m (flat-to-flat)	ULE segments w/ 7 DOF, ULE SM w/ 6 DOF
	Number of segments	36	Hex pack with center missing
	Segment width	1.315	meters (flat to flat)
	Collecting Area	53.912	meters
	Collected Photons / sec	5.39E+09	5th mag V-band star [500 - 600 nm]
	Coronagraphic Contrast	1.00E+10	at λ = 500 nm
	Inner Working Angle (IWA)	40	mas (3 λ/D at λ = 500 nm)
	Outer Working Angle (OWA)	640	mas (16 λ/D at λ = 500 nm) SFA or DM limited
	Diameter of cor hole	1280	mas
	Shear & K-mirror pupil rolls	12	during planet search, 1 during characterization
	End-to-End Optical Throughput	23%	OTE + VNC
	Full spectral passband	480 - 960 nm	Limited by 2X on fibers
	Instantaneous passband	<50%	Limited by phase plates and null control
	Spectroscopy	to R = 100 ?	In-band dispersive (ntegral field ?)
	Binary stars possible	Yes	53% G-stars are binary
	Resolved source	< 4 mas	Degrades null for stars > 4 mas diameter
	Pointing requirements	3.4 mas	3 sigma diameter
COARSE Control within OTE	Static OTE WFE (Difft'n Limited)	λ/14 rms = 35.71 nm rms	atλ = 500 nm
	OTE Coarse WFS&C	Sense: 1 nm rms WFE (3σ), Segm control: 5 nm rms WFE/segm (3σ) Segm Diff cntrl: 7 nm rms WFE/segm (3σ) Coarse control Δf: once per 5 min	Segment control is for piston, tip & tilt and assumed phase retrieval based w/ on-board closed-loop control. PSF Pickoff sensor following OTE + FMS but prior to VNC. Use out of science band photons for coarse control.
	Segm to Segm drift rate	5 nm (1σ) rms WFE / 5 min => 17 pm/sec	
	Segm to Segm overall diff	7.5 nm (1σ) rms WFE	
Fine Control within VNC	Controlled WFE (RMS)	< 25 pm rms	0-30 cpa NCP between nuller arms
	Segm to Segm drift rate	17 pm/sec	Shows up as NCP between nuller arms
	VNC Control bandwidth	0.1	Hz
	Total VNC WFE	76 pm	(Static 25 pm + Dynamic 3*17 pm)
	Coherent fiber bundle	1027 fibers	Length > 100μm, uselarge margin > 1 cm
	Deformable mirrors	2 - 1027 segmt	segm hex pack MEMS w/ 1027 piston/tip/tilt
	Total control DOF	6162	2 hex pack DMs with 3 DOF per DM segment
	Control spectral bandwidth	20	nm
	In-band control photon rate	2.48E+08	photons / control step in 10 nm passband
	Photon rate / control DOF	402458.20	photons / control step / DOF
	Photon limited sensing floor	62.72	pm per control DOF (assumes uncorrelated)

Table-1 shows the system level parameters, relevant to the coarse control of the OTE and fine control with the VNC.

2.2 OTE Wavefront Control

OTE wavefront control is accomplished in a manner similar to JWST and uses a focus diverse phase retrieval approach that has heritage to the Hubble Space Telescope (HST) and ultimately modified and verified[10] for use on the segmented telescope JWST. Light from a star (unresolved point source) passing through the OTE is fed to two WFS detectors after passing through selectable spectral filters to form two focus diverse images, i.e. images at different foci, of the star on the two separate detectors. Nonlinear iterative algorithms (aka phase retrieval) are employed on-board to invert the images and solve for the unknown wavefront errors. A pupil imaging lens is also employed in one of the WFS beam paths to create a pupil image (image of PM) to estimate the amplitude for the phase retrieval algorithms. The wavefront errors are subsequently decomposed into control modes of the OTE controllable DOF and converted to commands that are fed back to move the actuators on the PM segments and SM mirror. The baseline approach for ATLAST-9.2m is to operate in closed-loop on-board the spacecraft without operator intervention to maximize control bandwidth and minimize wavefront error. Nominal closed-loop OTE bandwidths are source brightness dependent but down to visual magnitude 19 stars still allow wavefront control every 5-10 minutes. The WFS instrument and overall approach is described in Feinberg et. al[11].

3. VISIBLE NULLING CORONAGRAPH FOR ATLAST-9.2M

3.1 Overview of Visible Nulling Coronagraph

The PM ATLAST-9.2m requires a coronagraph that works with segmented primary mirror. The VNC is one of the few options that will work with a segmented aperture telescope since it effectively works by destructively interfering light from one PM segment against another PM segment. In practice a group of four segments are interfered against each other in various combinations to use as many of the PM segments as possible to maximize throughput (figure-4). The VNC sky transmission function, without errors, is given by:

$$T(\theta_x,\theta_y)=\sin^2\left(\pi\frac{s_xD}{\lambda}\theta_x\right)\sin^2\left(\pi\frac{s_yD}{\lambda}\theta_y\right) \tag{1}$$

where (θ_x,θ_y) are the sky angles, λ and D are the wavelength and telescope diameter (D=9.2m) respectively and (s_x,s_y) are the fractional lateral beam shear in the x- and y-directions respectively. Thus a target star at $(\theta_x,\theta_y)=(0,0)$ has a transmission of 0.0, while a planet on the peak of the first transmission fringe at

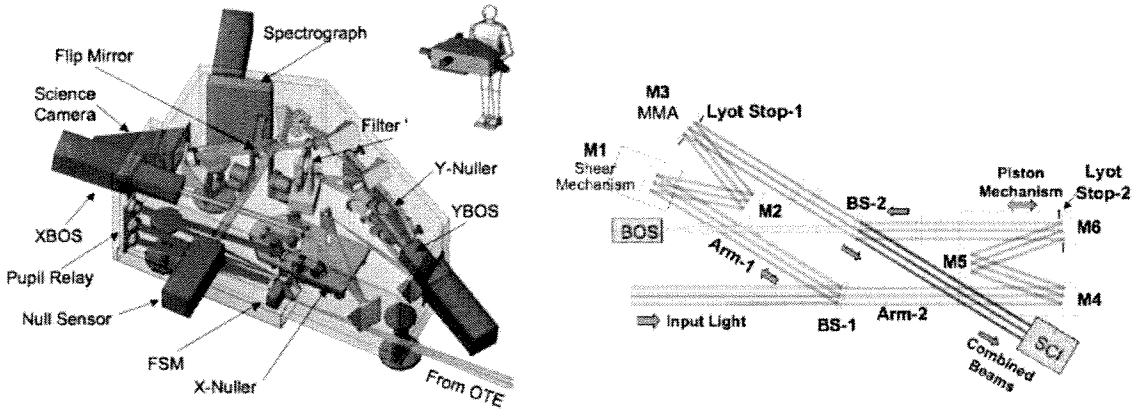

Figure-3: Left: Conceptual design of VNC. Right: Schematic of modified Mach-Zehnder nulling interferometer

$(\theta_x,\theta_y)=\left(\frac{1}{s_x},\frac{1}{s_y}\right)\frac{\lambda}{2D}$ has unit transmission monochromatically. The inner working angle (IWA) is taken to be at the location of the first transmission maxima and gives an IWA of $\theta_{IWA}=\sqrt{\frac{1}{s_x^2}+\frac{1}{s_y^2}}\frac{\lambda}{2D}$. For ATLAST-9.2m, shearing of 2 aperture segments in X, out of 7 across its diameter, 1.74 segments in Y (due to the hexagonal pack pupil geometry) yields a limiting IWA of $\theta_{IWA}=2.67\lambda/D=33$ mlli-arcseconds (mas) which implies that wavefront and amplitude spatial frequency structure at and near ~2.7 cycles per aperture are the most critical spatial frequencies to sense and control.

3.2 VNC Optical Design Description

The ATLAST flight VNC would consist of two nullers in series as shown for one possible design in the left panel of figure-3. Light from the optical telescope element (OTE) enters and passes through a relay with a fine steering mirror and enters the 1st nuller (orange 6 sided optical bench near center of figure-3 and the dark output is relayed to the 2nd nuller (orange 6-sided optical bench on the right wall). Each nuller is a modified Mach-Zehnder interferometer as shown schematically in the right panel of figure-3.

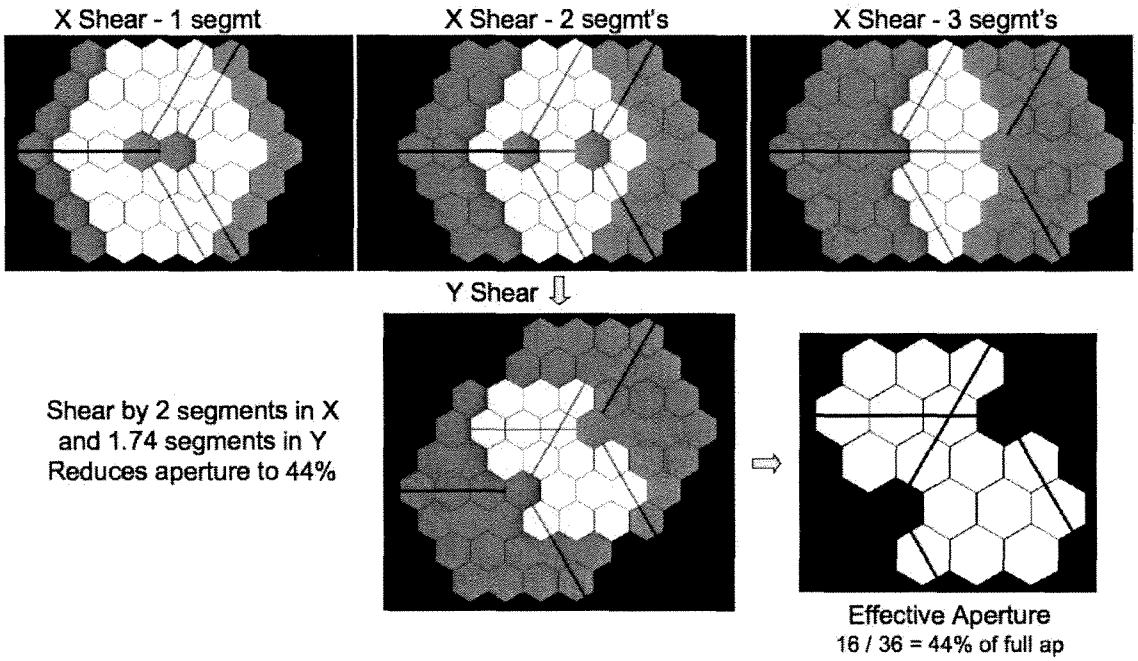

Figure-4: Effect of Shearing ATLAST-9.2m Aperture. Top Row left-to-right: Shear by 1,2 & 3 PM segments, white regions are effective aperture after shear. Bottom center: Shear of 2 segment widths (flat-to-flat) in X followed by shear of 1.74 segment widths in Y. Effective aperture after X/Y shear is 44% of full aperture ,shown on lower right.

The input light to each nuller is 50:50 split by beamsplitter-1 and passes through the two arms (arm-1 and arm-2). Arm-1 reflects off the 1st beamsplitter while arm-2 transmits. In arm-1 the beam reflects off 3 flat optics (M1,M2,M3) of which M1 is mounted on a shear mechanism that moves in 1 degree of freedom (DOF) normal to the incoming beam. The shear mechanism laterally translates the beam in arm-1 relative to arm-2. M2 folds the beam onto the Multiple Mirror Array (MMA) (mirror M3), shown in Figure-6, at near normal incidence. Herein we refer to the deformable mirror as the MMA to differentiate it from continuous facesheet deformable mirrors. After the MMA, the beam both reflects and transmits off beamsplitter-2 which is matched to the transmission/reflection characteristics of beamsplitter-1. The reflected beam passes out to the bright object sensor (BOS) and the transmitted to the science output (SCI). The high contrast science output is the dark output, and when nulled, most of the light passes to the BOS. The light which transmits through beamsplitter-1 also reflects off fold flats M4, M5 and M6 as shown to the right of figure-3. M4, M5 and M6 are all mounted on a single 1 degree of freedom (DOF) two-stage

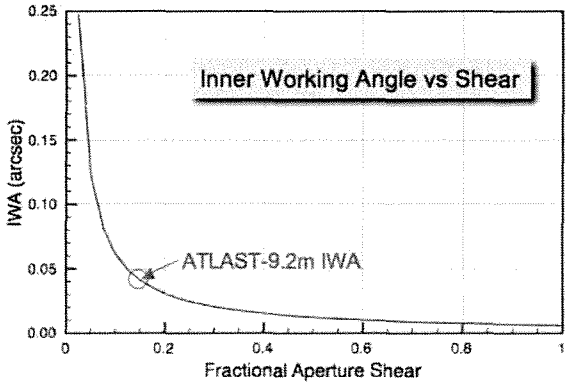

Figure-5: Inner Working Angle vs. Fractional Aperture Shear in X and Y

actuation assembly (piston mechanism) that moves to maintain the mean phase difference between arm-1 and arm-2 at π radians at the center wavelength. Light from arm-2 also transmits and reflects off beamsplitter-2 and is mixed against the beams from arm-1. Just in front of the MMA and its counterpart in arm-2 are Lyot stops 1 & 2 that are matched to each other and to the pattern of the MMA and insures that the Fresnel diffraction within the two arms matches. At the output of the bright and dark arms are relay optics (not shown) that relays the beams onto the bright and dark detector arrays. For the flight nuller the dark output is collimated and relayed to the 2nd nuller which is a duplicate of the first except it is rotated 90 degrees about the optical axis of the output beam. The bright outputs are used for wavefront sensing and control and contain interferogram images of the PM. The final dark output contains the coronagraphic in-focus image.

To achieve the inner working angle (IWA) the pupil image must be *sheared*, i.e. one arm of nuller is translated relative to the other arm prior to the beams being recombined as shown in figure-4. The shear must be integral units of the width of the a single PM segment. This effectively mixes one segment of the PM against another. The 1st nuller shears in the X-direction, and the second in the Y direction. The region of common pupil overlap is masked by a Lyot stop. The shearing reduces the effective aperture with more shear yielding smaller effective aperture and hence throughput, however, larger shears gives a better IWA.

4. WAVEFRONT CONTROL

4.1 Effect of Wavefront Error on Contrast

Differences in wavefront, amplitude, and polarization between the sheared segments all contribute to a reduction in contrast since the fields no longer perfectly subtract between a given set of 4 segments, i.e. that set of 4 which are sheared in the pupil to overlap. It is the difference in these terms which cause leakage and error budgeting, sensing and control are designed to control this difference. This is different from most other types of coronagraphs since in that they require absolute control of these errors.

For example figure-6 shows a simulation of the effect of random wavefront error. The upper left shows a random realization of the σ = 0.055 nm rms differential wavefront error, where differential refers to differences between the sheared segments and includes random piston, tip, tilt and a single realization of a random PSD of the form of ~$1/f^3$, it does not include differential reflectivity nor polarization errors or pointing errors. The top right of figure-6 shows the residual or leakage point spread function (PSF), and the lower plot in figure-6 shows the effect of scaling the differential rms wavefront error. To achieve an IWA of 40 mas requires σ ~ 0.055 nm rms differential wavefront error between the sheared segments. However this is for a static case, i.e. without drift and closed-loop control.

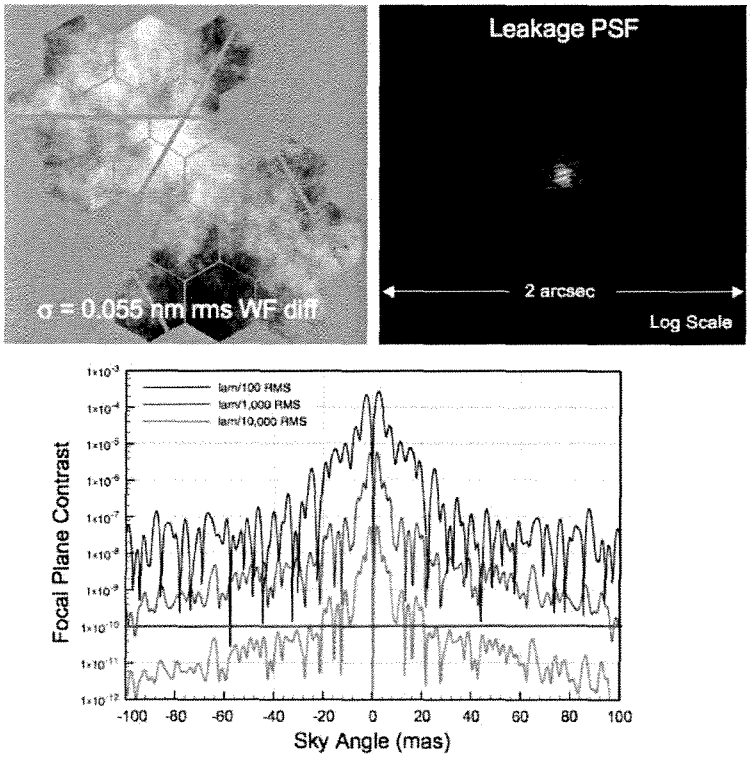

Figure-6: Effect of differential wavefront error on leakage PSF. Upper left: random realization of differential WFE. Upper right: Resulting leakage PSF that leaks through VNC. Bottom: Effect of scaling the differential WFE.

4.2 Wavefront Sensing

As previously discussed the OTE wavefront sensing is performed by the use of phase retrieval methods used for JWST[10,11]. Within the instrument the finer wavefront sensing is accomplished by looking at the interferometric image from the bright output arms of the nuller, and from the science image from the dark output arm of the 2nd nuller. This approach is currently undergoing validation as part of a NASA funded Technology Development for Exoplanet Missions (TDEM) effort[3] and is further detailed in reference 3. Results of this TDEM effort will be available in the fall of 2010.

4.3 Basis of Error Budgeting Formalism

Consider only a single nuller with a bright and dark output channel. The noise free image irradiances in the single nuller's bright and dark focal planes are given by:

$$\begin{cases} I_B(\theta) = \frac{1}{2} I_1 PSF_0(\theta) + \frac{1}{2} I_2 PSF_\phi(\theta) + \sqrt{I_1 I_2}\,\mathrm{Re}\left\{ASF(\theta) ASF_\phi^*(\theta)\right\} \\ I_D(\theta) = \frac{1}{2} I_1 PSF_0(\theta) + \frac{1}{2} I_2 PSF_\phi(\theta) - \sqrt{I_1 I_2}\,\mathrm{Re}\left\{ASF(\theta) ASF_\phi^*(\theta)\right\} \end{cases} \tag{2}$$

where $I_B(\theta)$ and $I_D(\theta)$ represent the bright and dark channel output images, θ is the angular variable representing the focal plane projected on the sky, and where $I_1 + I_2 = I_{STAR}$. I_{STAR} is the integral over sky angle of the stellar flux collected by ATLAST. I_1 and I_2 are the beamsplitter reflected and transmitted fluxes. PSF represents the optical point spread function of the Lyot stopped pupil, including the beam shear, and the subscript '0' represents the unaberrated PSF and the subscript 'φ' represents the aberrated (phase and/or amplitude) PSF. Both PSFs are normalized such that their integrals over $d\theta$ are unity. ASF is the complex amplitude spread function such that $PSF = |ASF|^2$. It is straightforward to show that $I_B(\theta) + I_D(\theta) = I_1 PSF_0(\theta) + I_2 PSF_\phi(\theta)$ and thus the integral of this sum is $I_{STAR} = I_1 + I_2$. The phase and amplitude aberrations can be ascribed to one arm or the other of the interferometer without loss of generality since it is only differences that ultimately matter.

Expanding the dark channel equation (2nd equation in (2)) using the small angle approximation for the phase error, i.e. $e^{i\phi} \approx 1 + i\phi$, results in the contrast relation that $C = \frac{I_D}{I_{STAR}} \approx \left(\frac{\pi W_0}{\lambda}\right)^2 PSF_0(\theta - \theta_0)$ where θ_0 is the location of the planet and W_0 is the wavefront error amplitude at one given spatial frequency. If the mean wavefront error is zero (equivalent to piston difference between nuller arms being zero) then the average contrast is $\langle C \rangle \approx \left(\frac{\pi W_0}{\lambda}\right)^2$. The brightness of speckles is exponentially distributed such its mean is equal to the standard deviation of its intensity, and, since we desire to set the requirements for the VNC based on high confidence statistics we require $\langle C \rangle + 3\sigma_{\langle C \rangle} = 4\langle C \rangle \le C_{FLIGHT}$ where C_{FLIGHT} is the flight requirement limit. This insures that the flight contrast limit will be met better than 99% of the time. Solving the contrast equation for a single spatial frequency wavefront term gives $W_0 \approx \frac{\lambda}{2\pi}\sqrt{\langle C \rangle}$ per spatial frequency. Thus the rms of this term is $W_{RMS} \approx \frac{1}{\sqrt{2}}\frac{\lambda}{\pi}\sqrt{\langle C \rangle}$ per spatial frequency.

For a VNC operating at C=10^{-10} at λ=500 nm requires $W_{RMS} \approx 0.0011$ nm rms per spatial frequency. The overall rms wavefront error (WFE) is obtained by integrating W_{RMS}^2 over all spatial frequencies of interest. Spatial frequencies of interest are limited to that which is controllable by the deformable mirror (DM). The DM would have 1027 hex pack segments, and each of which has 3 control degrees of freedom (DOF) for 3081 control DOF in all. The number of control DOF across the diameter of the beam is given by $\sqrt{\frac{\pi}{4} DOF} \approx 50$ and Nyquist sampling (2 per spatial frequency period) gives correction out to 25 cycles per beam. Using W_{RMS}^2 as the circular PSD, with random phase (white noise assumption) and integrating over the 2D spatial frequencies of interest gives $\sigma_{WFE} = \frac{\lambda}{4}\sqrt{\frac{DOF \cdot \langle C \rangle}{2}}$ for the rms WFE. To achieve contrast of 10^{-10} with 3081 DOF at λ=500 nm requires $\sigma_{WFE} \leq 0.049$ nm rms WFE where this is the rms difference of the wavefront error between the two arms of the nuller after DM control, and, if all other error sources are considered negligible. However amplitude, polarization and pointing induced beam walk as well as point errors will contribute.

Amplitude errors are handled in a fashion similar to the above and equivalent type expressions can be derived for both amplitude and polarization tolerances before and after sensing and control.

4.4 Error Budget after Sensing and Control

Table-2: Error Budget after Sensing and Control

Contributor	Value	Units	Contribution to Pupil Plane Null
Uncorrected Piston Difference (rms)	0.002	nm	1.58E-10
Differential Beam Tilt (rms)	0.002	mas	3.93E-08
Uncorrect WFE (rms)	0.020	nm	1.61E-08
Uncorrected Reflectivity Errors	0.001	%	6.25E-12
Differential Polarization	0.001	deg	7.62E-11
	End Pupil Plane Null =		**5.56E-08**
	Focal Plane Contrast =		**1.00E-10**

Table-2 shows a top level error budget after sensing and control. It is broken out into 5 terms. Uncorrected piston difference is the rms of uncontrolled differences in only the piston between the 4-sheared segments. Differential beam tilt is the uncontrolled rms difference in tip/tilt of the 4 segments in units of milli-arseconds of the segment in the telescope entrance pupil, i.e. at the PM. Uncorrected WFE is the uncontrolled difference wavefront error between the 4 segments without piston or tip/tilt, i.e. with piston and tip/tilt differences removed. Uncorrected reflectivity errors are the uncorrected variation in reflectivity across the set of 4 shear combined segments, in relative units, i.e. assuming a unit amplitude plane wave at the telescope entrance aperture. Note that this is after correction via using either 2 DMs or using a single DM a passive fiber bundle corrector. Differential polarization is the rms rotation angle difference of the polarization state after reflecting off all the optics and passing through the VNC and is in units of degrees of rotation. Each of these are 1-sigma numbers and each contributes to a loss in pupil plane null depth. Converting from pupil plane null depth to contrast is accomplished by using $C \approx \frac{Null}{1+\frac{\pi^4}{8}\theta_{IWA}^3}$ where θ_{IWA} is in units of λ/D and where 40 mas has been assumed. Strictly speaking this makes an implicit, but reasonable, assumption on the slope of the power spectral density of the errors that is adequate for error budgeting but needs further verification for real world optics and deformable mirrors. Table-2 shows that with allocations shown that 10^{-10} can be achieved if the values in the 2nd column can be met.

5. SUMMARY

ATLAST-9.2m could achieve exoplanet science for terrestrial planets, to IWA ~40 mas, with a segmented aperture system without the need to develop very large lighweighted monolithic space optics. The segmented mirror development has legacy to JWST mirror development, and the OTE wavefront control approach has been validated on the ground for JWST, and, pending launch of JWST will become part of the routine maintenance of JWST. The VNC and its associated

technologies have been steadily advancing and is currently funded for a 2-year effort to advance the NASA technology readiness levels to TRL-5. Preliminary error budgeting shows that tolerances are difficult but comparable to that of TPF-C, however, ATLAST-9.2m could achieve a wider breadth of science.

REFERENCES

[1] Postman, M. et. al.., "Advanced Technology Large-Aperture Space Telescope (ATLAST) - Technology Roadmap for the Next Decade", NASA Astrophysics Strategic Mission Concept Study, (2009), available from http://www.stsci.edu/institute/atlast.

[2] Lyon, R.G., Heap, S., Lo, A., Cash, W., Starkman, G., Vanderbei, R., Kasdin, J., Copi, C., "Externally Occulted Terrestrial Planet Finder Coronagraph: Simulations and Sensitivities", Proc. SPIE 6687, San Diego, (2007)

[3] Lyon, R. G., Clampin, M., Shao, M., Woodruff, R. A., Vasudevan, G., Melnick, G., Tolls, V., Petrone, P., "Nulling coronagraphy for Exo-Planetary Detection and Characterization," Proc. IAU #200, Nice France, (2005)

[4] M. Clampin, R. Lyon, EPIC Science Team, *The Extrasolar Planetary Imaging Coronagraph*, Pathways Towards Habitable Planets, Barcelona Spain, Sept 14-18, (2009)

[5] Clampin, M., Melnick, G., Lyon, R., Kenyon, S., Sasselov, D., Tolls, V., Ford, H., Golimowski, D., Petro, L., Hartig, G., et. al, "Extrasolar planetary imaging coronagraph (EPIC)," Proc of SPIE 6265, (2006)

[6] Shao, M., S. Bairstow, E. Deems, L. Fletcher, B.M. Levine, G. Orton, G. Vasisht, L. Wayne, F. Zhao, M. Clampin, R. Lyon, O. Guyon, B. Lane, K. Harvey, J. Wynn, R. Samuele, G. Vasudevan, R. Woodruff, V. Tolls, F. Malbet, A. Leger, "A Mission Concept Study of a Dilute Aperture Visible Nulling Coronagraph Imager (DAViNCI) for the Detection and Spectroscopy of Exo-planets", AAS, (2010)

[7] Lyon, R. G., Clampin, M., Woodruff, R. A., Vasudevan, G., Thompson, P.., Petrone, P., Madison T., Rizzo, M., Melnick, G., Tolls, V., "Visible nulling coronagraph testbed results," Proc. SPIE 7440, (2009).

[8] Lyon, R. G., Clampin, M., Woodruff, R. A., Vasudevan, G., Thompson, P., Chen, A., Petrone, P., Booth, A., Madison T., Bolcar, M. R., Melnick, G., Tolls, V., "Visible nulling coronagraphy testbed development for exoplanet detection," Proc. SPIE 7731, (2010).

[9] B.M. Levine, F. Aguayo, J. Chapsky, I. Cheung, S. Crawford, A. Dingizian, R. Gappinger, A. Eisenman, P. Irwin, T. Lockhart, P.R. Lawson, J.S. Sandhu, M. Shao, J. Shaw, T.J. Shen, R. Smythe, J. Wu, R. Zimmer, R. Samuele, F. Malbet, M. Clampin, R. Lyon, "Advanced Visible Nulling Coronagraph Test Bed Facility", AAS, (2010)

[10] Dean, B., et. al., "Phase Retrieval Algorithms for JWST Flight and Testbed Telescope", Proc. SPIE 6265 (2006).

[11] Feinberg, L. et. al, "Large Segmented UV-Optical Space Telescope Using a Hybrid Sensor Active Control Architecture", Proc. SPIE 7436 (2009).